Dynamics of the particle morphology during the synthesis of waterborne polymer-inorganic hybrids

*Shaghayegh Hamzehlou; Miren Aguirre; Jose R. Leiza; José M. Asua**

POLYMAT, Kimika Aplikatua saila, Kimika Zientzien Fakultatea, University of the Basque Country UPV/EHU, Joxe Mari Korta Zentroa, Tolosa Hiribidea 72, 20018 Donostia-San Sebastián, Spain

Corresponding Author

*Email: jmasua@ehu.es

Abstract

Waterborne polymer-inorganic hybrids have the potential of both surpassing the performance and targeting applications that are out of reach of conventional polymer dispersions. The properties of these hybrids are determined by the particle morphology achieved during the synthesis. In this work, the evolution of the particle morphology during the polymerization of (meth)acrylate monomers in the presence of CeO_2 was determined by cryo-TEM. Moreover, a mathematical model for the dynamics of the particle morphology during the synthesis of polymer-inorganic hybrids was developed and its capabilities checked against the experimental data. It is our hope that this study will help to further elucidate the mechanism involved in the process and to lay the foundations for a fine control of particle morphology of these materials.

Keywords: Particle morphology, hybrid polymer-inorganic particles, miniemulsion polymerization

Introduction

Waterborne polymer-inorganic hybrids have attracted plenty of attention because in addition to the improvement of the performance in established applications, they allow targeting new applications that are out of reach of the conventional waterborne polymer latexes.[1] In terms of particle morphology, the waterborne polymer-inorganic hybrids can be classified in particles with the inorganic material at the surface, single particles encapsulated by polymer and particles containing multiple encapsulated inorganic particles.

The inorganic particles at the surface of the particles have two positive effects. On one part, they improve the mechanical properties of the film[2–5]and on the other hand, they can stabilize the particles avoiding the use of surfactants that increase the water sensitivity of the films.[4–8] The challenge in these hybrids is to prepare dispersions with solids contents in the range of commercial latexes (≥50 wt %) with modest amount of inorganic material and minimizing the fraction of inorganic material in the aqueous phase. Both emulsion[6,9,10] and miniemulsion[4,5,11,12] polymerization can be used to synthesize polymer-inorganic hybrids with the inorganic particles at the surface of the particles, but only miniemulsion polymerization has been able to fulfil the conditions given above.[4,5] For this process, the morphology of the hybrid particle does not really evolve (other than the effect of the formation of polymer and the partitioning of the inorganic material between the surface of the particles and the aqueous phase).

Encapsulation of single inorganic particles is achieved by seeded emulsion polymerization in which the inorganic particles acts as seed. A delicate balance of the reaction conditions is needed to avoid both nucleation of polymer particles devoid of inorganic material and aggregation of particles.[13–15]Under these circumstances the evolution of the morphology is limited to the shape of the polymer attached to the particles that create lobes[15] or a continuous shell.[13,14]

Polymer-inorganic hybrids in which the inorganic particles are embedded within the polymer show a wide variety of morphologies [16–19] and this article is devoted to them.

The equilibrium morphologies of polymer-inorganic hybrids have been calculated by minimizing the surface energy of the system; leading to a map of morphologies as a function of the ratio between the interfacial tensions.[20] The map has been used to explain the changes in morphology caused by variations in the type of initiator[21,22], surfactant concentration[17] and type of monomer.[22]

An intrinsic limitation of this approach is that it only considers the equilibrium morphology and by similarity with the case of polymer-polymer waterborne hybrids, it is expected that morphology is determined by the interplay between thermodynamics and kinetics. This implies the study of the evolution of polymer-inorganic particles, which is a subject basically not covered in the literature. Aguirre et al. [23,24] partially addressed this problem by mimicking the polymerization by preparing miniemulsion droplets containing CeO_2 particles and different monomer/polymer ratios, but although enlightening, the study provides only the equilibrium morphologies for the different compositions of the particles.

In this work, the dynamic evolution of the morphologies of waterborne polymer-

inorganic hybrids is investigated. Using an acrylic/CeO_2 system as case study, the evolution of the particle morphology was experimentally determined. Then, a mathematical model for dynamics of the morphology of waterborne polymer-inorganic hybrids was developed and its capabilities tested with the experimental data.

Experimental part

Materials

The hydrophobically modified CeO_2 dispersion (Altana, Germany) was received in mineral spirits (49 wt%) and it was dried at 60°C for 2 days before use. The modifier that makes them dispersible in organic media[19,25] is proprietary of the company and its characteristics are not disclosed. Nevertheless, some information about the CeO_2 nanoparticles can be deduced. In order to be efficient in organic media the modifier should provide steric stabilization, namely the CeO_2 nanoparticles wee likely covered by a hairy layer compatible with the monomers (Flory-Huggings interaction parameter smaller than 0.5). The size of the individual particles as measured by TEM was 3 nm (Figure S1, Supporting Information) MMA (Quimidroga), n-Butyl acrylate (BA; Quimidroga) and acrylic acid (AA ;Aldrich) were used as received. The initiator, potassium persulfate (KPS, Aldrich) was used as supplied. Dodecyl diphenyloxide disulfonate (Dowfax 2A1, 45 wt%, Dow Chemicals) and n-Octadecyl acrylate (stearyl acrylate, 97 wt%, Aldrich) were used as anionic emulsifier and costabilizer, respectively. Deionized water (MiliQ quality, MiliPore) was used throughout the work.

Miniemulsion Preparation

The miniemulsions were prepared using the formulation given in Table 1. First, CeO_2 nanoparticles (2 wbm% with respect to the monomers forming the organic phase) were

dispersed in the monomer mixture under magnetic stirring for 15 min at 800 rpm. The dispersion was mixed with an aqueous solution of the emulsifier (Dowfax 2A1) and stirred magnetically for 15 min. The coarse emulsion was sonicated in a Branson Digital Sonifier 450/SEE-1 for 15 min (operating at 8-output control and 80% duty cycle) in an ice bath under magnetic stirring. A stable miniemulsion was obtained.

Table 1. Formulation used to prepare the miniemulsion at 40 wt% solids content.

	Component	**wt %**
Organic Phase	MMA	19.8
	BA	19.8
	AA	0.4
	Stearyl Acrylate*	4
	CeO_2*	2
Water Phase	Dowfax*	2
	Water	60

*With respect to the monomers

Polymerization of the hybrid latexes

Batch miniemulsion polymerizations were carried out in a commercial calorimetric reactor (RTCal™, Mettler-Toledo), consisting of a 1 L glass jacket reactor vessel, an anchor agitator, platinum resistance thermometer, a nitrogen inlet and a sampling tube. The hybrid miniemulsion was loaded into the reactor, purged with nitrogen for 30 minutes, and heated to the reaction temperature (60 °C) under constant agitation of 150 rpm. After equilibration of the temperature, the initiator (KPS 0.15 wbm% , weight percent based on monomer) was added in a single shot. Samples were taken periodically

and short stopped with hydroquinone. The samples were kept in refrigerator for 24 h before morphology analysis.

Characterization

Conversion was measured by gravimetry. Particle morphology was determined by Cryo-TEM and for the preparation of the samples one drop of the sample (~3 μl) was deposited in a copper grid (300 mesh, R QUANTIFOIL® R 2/2 EMS, Hat-field, PA, USA, hydrophilized by glow-discharged treatment just prior to use) within the environmental chamber of a FEI Vitrobot Mark IV (Eindhoven, The Netherlands) and the excess liquid was blotted away. The sample was introduced into melting (liquid) ethane and transferred to a Single Tilt Cryo-Holder. The Cryo-Holder was previously prepared by 655 Turbo Pumping Station to maintain the sample below –170°C and to minimize the thermal derive. The sample was examined in a TECNAI G2 20 TWIN (FEI, Eindhoven, The Netherlands) microscope, operating at an accelerating voltage of 200 kV in a bright-field and low-dose image mode.

Evolution of particle morphology

Figure 1 presents the evolution of the particle morphology. For convenience, the map of equilibrium polymer-inorganic particle morphologies is used as a reference, but it should be stressed that most of the morphologies observed were not at equilibrium. It can be observed that the CeO_2 particles (dark dots) were well dispersed inside the initial miniemulsion droplets. This is a CeO_2-in-monomer-in-water double dispersion. In terms of relative positions of the CeO_2 particles, monomer and water, this is an equilibrium morphology. The dispersion of the CeO_2 particles in the monomer indicates that the interfacial tension between the inorganic material and the monomer, γ_{IP}, is low (the

subscript P is used for the monomer/polymer organic phase). Therefore, γ_{IP}/γ_{PW} (γ_{PW} being the interfacial tension between the organic and the aqueous phase) was lower than 1. On the other hand, the fact that the surface modified CeO_2 particles were within the monomer droplets indicated that the interfacial tension between them and water (γ_{IW}) was high. Therefore, $|\gamma_{PW} - \gamma_{IP}|/\gamma_{IW} < 1$, which means that the position of the CeO_2 containing monomer droplets should be in the region of the map represented by a core of inorganic particles separated from water by a shell of monomer. The CeO_2 particles were sterically stabilized within the droplets.

At 1% conversion, Figure 1 shows a severe destabilization of the CeO_2 particles within the droplet/particle. The cause of the destabilization may be depletion flocculation and/or incompatibility between the newly formed polymer and the steric stabilizer of the CeO_2 that led to a contraction of the hairy layer of the stabilizer. Consequently, the CeO_2 particles could approach to a distance in which the van der Waals forces were important and some coagulation occurred. It is worth pointing out that the concentration of CeO_2 in the small particles was higher than in the large ones because of the Ostwald ripening.[26,27] The reason is that miniemulsification leads to a broad droplet size distribution and because of interfacial tension, the chemical potential of the monomer in the small droplets is higher than in the large ones. Consequently, monomer diffuses from small to large droplets. This leads to an increase of the concentration of CeO_2 nanoparticles in the small droplets. Complete diffusion of the monomer is avoided by the costabilizer (stearyl acrylate).

At 8% conversion, massive coagulation was evident and the aggregates formed moved to the surface of the particle. The reason for the formation of aggregates was the

additional contraction of the hairy layer, which still provided some steric stabilization because the CeO_2 particles did not form compact aggregates. The movement of the aggregates can be explained considering the equilibrium morphology map. As the fraction of polymer in the particles increased, the interfacial tension between the inorganic particles and the organic phase increased, and therefore the equilibrium morphology evolved following the solid arrow crossing to the region of the hemispherical equilibrium morphology. Clearly, the morphologies observed at 8% conversion were not at equilibrium because the particles contained a variety of aggregates in non-equilibrium positions. At 18% conversion, the aggregates were more compact.

At 40% conversion, the trends observed before were enhanced, but still some particles presented non-equilibrium morphology as they contained more than one aggregate. The aggregates were more compact suggesting further contraction of the hairy layer around the CeO_2 particles. It is worth pointing out that the path illustrating the equilibrium morphologies passes through $\frac{|\gamma_{PW}-\gamma_{IP}|}{\gamma_{IW}} = 0$ when $\frac{\gamma_{IP}}{\gamma_{PW}} = 1$.

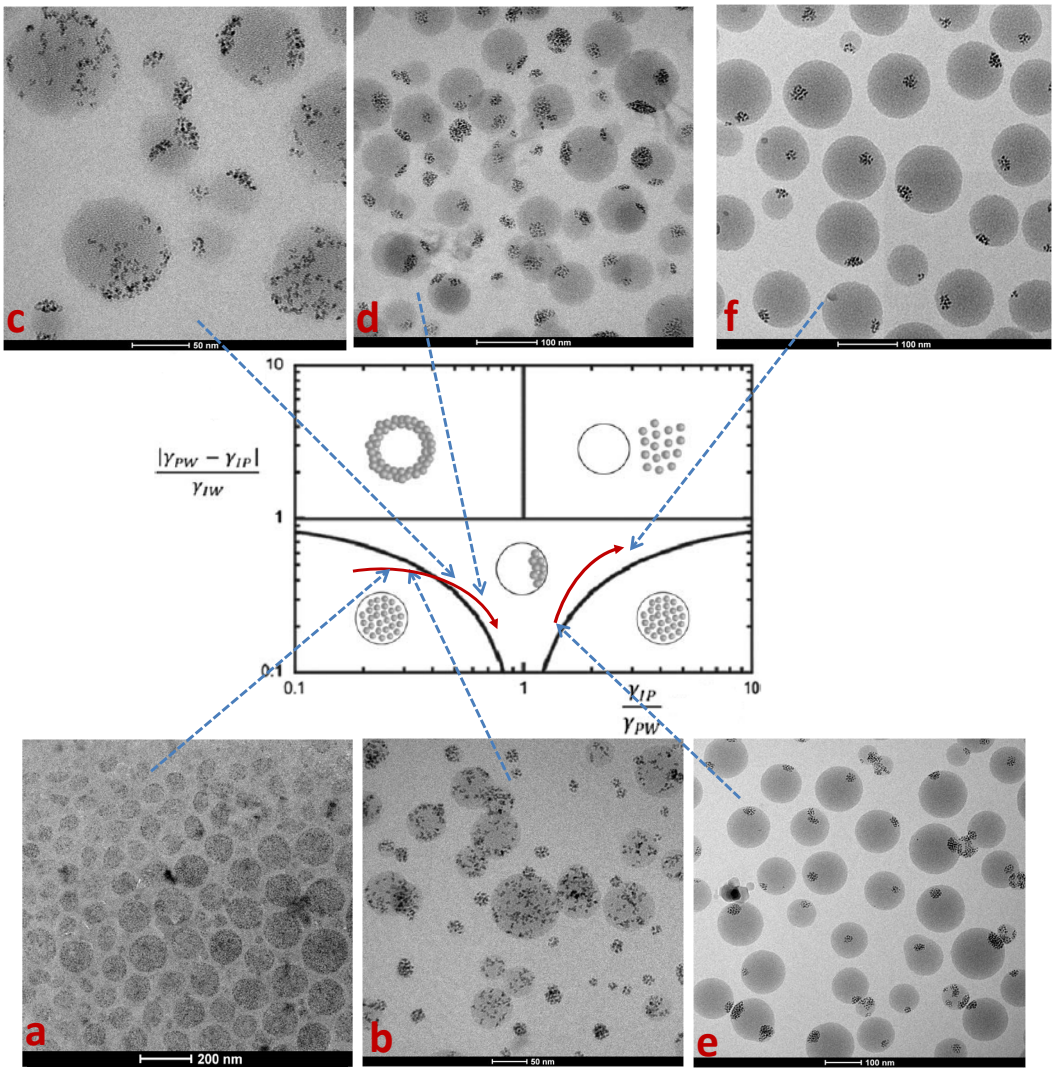

Figure 1. Evolution of the particle morphology for a) monomer-CeO_2 droplets, b) 1% monomer conversion, c) 8% monomer conversion, d) 18% monomer conversion, e) 40% monomer conversion and f) 100% conversion.

Finally at 100% conversion, there was a single compact aggregate per particle located at the surface of the particles, which corresponds to an equilibrium morphology. At first sight it seems that the amount of CeO_2 per particle is lower than at lower conversions, suggesting that some particles were expelled to the aqueous phase (which could be caused

by a large increase in γ_{IP} that makes the system to cross to the upper right region). However, no traces of CeO_2 particles were found in the serum and the average number of CeO_2 nanoparticles per polymer particle estimated from the size of aggregates (22 nm, assuming that the CeO_2 formed a compact aggregate) was 252 which agrees well with the amount of CeO_2 used in the formulation. (See Supporting Information for details of the calculation).

Modeling the dynamic evolution of the morphology of water-borne polymer-inorganic hybrids

The results discussed in the previous section tremendously improve the understanding of the processes controlling the morphology of the waterborne polymer-inorganic hybrids, but if a different morphology were sought, extensive experimental work would be still needed. Further work would be necessary to determine the optimal strategy to produce the sought morphology (e.g. the strategy that minimizes the reaction time). A mathematical modelling can reduce the experimental effort needed to determine the optimal strategy to produce a given morphology. In addition, due to the lack of devices for on-line monitoring of the particle morphology, mathematical models are needed for the practical implementation of the optimal strategy. [1]

In this section, for the first time, a mathematical model for the dynamics of the particle morphology of waterborne polymer-inorganic hybrids is presented.

The model is inspired by the one developed by Hamzehlou et al. for polymer-polymer waterborne hybrids.[28] The basic idea is that the particles of an aqueous dispersion have different morphologies (see Figure 1) and that this variety can be characterized by a distribution of aggregates (similar to the characterization of a polymer by the molecular

weight distribution or a colloid by the particle size distribution). In addition, distinction is made between the aggregates at equilibrium and non-equilibrium positions, where equilibrium refers to the equilibrium morphology at 100% conversion. More specifically for the case in Figure 1, where the final equilibrium morphology is hemispherical, the particles observed at 8% conversion were not equilibrium morphologies, but the aggregates located at the surface were at equilibrium positions, whereas those placed inside of the particle were not at equilibrium positions. Population balances for a non-equilibrium and equilibrium positions were developed. For a hemispherical equilibrium morphology, the population balance for clusters at non-equilibrium positions is as follows:

$$\frac{dm(v)}{dt} = \left(1 - \delta_{v \le 2v_c}\right)\alpha_m(v)\frac{k_a}{V_p}\left(1 - \frac{1}{m_{av}}\right)\int_{v_c}^{v-v_c} m(u)m(v-u)du$$

(Generation by coalescence of aggregates)

$$-2m(v)\frac{k_a}{V_p}\left(1 - \frac{1}{m_{av}}\right)\int_{v_c}^{v_{max}-v} \alpha_m(v+u)m(u)\,du$$

(Disappearance by coalescence of aggregates)

$$-k_{mov}m(v) \qquad (1)$$

(Movement to equilibrium)

where $m(v)$ is the number of aggregates that are at non-equilibrium positions and contain v inorganic particles. The first term of the right hand-side of equation 1 accounts for the formation of aggregates of size v by aggregate coalescence, and the second and third terms account for the disappearance of aggregates of size v by coagulation and transfer to the equilibrium positions, respectively. Implicit in this

term is the assumption that the aggregates are irreversibly formed (the inorganic particles do not leave the aggregates). v_c is the minimum number of inorganic particles in one aggregate and v_{max} is the maximum number of inorganic particles per hybrid particle, that was considered to be twice the average number of inorganic particles per hybrid particle:

$$v_{max} = 2v_{av} = \frac{2v_{tot}}{\mathrm{N_p}} \tag{2}$$

where v_{tot} is the total number of inorganic nanoparticles in the formulation. To avoid the coagulation of big aggregates that may exceed the maximum aggregate size and to decrease the probability of coagulation of big aggregates with sizes higher than the average value, a probability, $\alpha_m(v)$, in the form of an exponential decay function was defined as:

$$\alpha_m(v) = \begin{cases} 1 & if\, v_c < v < (v_{\mathrm{av}} - \bar{v}_n) \\ \exp\left(-\frac{\propto^*(v-(v_{\mathrm{av}}-\bar{v}_n))}{v_{av}}\right) & if\ (v_{\mathrm{av}} - \bar{v}_n) < v < v_{max} \\ 0 & if\ v > v_{max} \end{cases} \tag{3}$$

where $\bar{v}_n$ is the average number of inorganic particles in aggregates at equilibrium positions. Furthermore, the term $\left(1 - \frac{1}{m_{av}}\right)$ insures that the coagulation rate approaches to zero as the average number of aggregates at non-equilibrium positions per particle m_{av} approaches one. Note, that δ is equal to one if the condition in its subscript is fulfilled (i.e. $\delta_{v \le 2v_c} = 1$ if $v \le 2v_c$).

The coagulation constant between two aggregates, k_a, was assumed to be proportional to the terminal velocity created by the van der Waals attraction forces

between them[29].

$$k_a(u,v) \div \frac{F_A}{\eta}\left(\frac{1}{r_u}+\frac{1}{r_v}\right) \quad (4)$$

where η is the internal viscosity of the particle and r_i the hydrodynamic radius of the aggregate. On the other hand the van der Waals attraction force between two spherical aggregates is a function of the sizes of the aggregates[30]:

$$F_A \div {}^{r_u r_v}/_{r_u + r_v} \quad (5)$$

which gives:

$$k_a(u,v) \div {}^{1}/_{\eta} \quad (6)$$

The viscosity in concentrated[31] and diluted[32] polymer solutions is given by:

$$\eta \div \ {\phi_P}^5 * \exp\left(k_\eta\left(\frac{T_g}{T}-1\right)\right) \qquad \phi_P > 0.1 \quad (7)$$

$$\eta \div \ \exp\left(k_\eta\left(\frac{T_g}{T}-1\right)\right) \qquad \phi_P < 0.1 \quad (8)$$

where ϕ_P is the volume fraction of the polymer, k_η is the activation energy for viscous flow and T_g is the glass transition temperature of the polymer-monomer mixture given by:[33]

$$T_g = \frac{T_{gP} + (kT_{gM} - T_{gP})\phi_M}{1 + (k-1)\phi_M} \quad (9)$$

where T_{gP} and T_{gM} are the glass transition temperatures of polymer and mixture of monomers, respectively, ϕ_M is the monomer fraction in the matrix, and k is a constant varying from 1 to 3.

Combination of equations 4-8 leads to:

$$k_a = \frac{k_{a0}}{{\phi_P}^5 * \exp\left(k_\eta(\frac{T_g}{T} - 1)\right)} \quad (10)$$

The last line of equation 1 includes the term linked to the movement of aggregates from non-equilibrium to equilibrium positions characterized by the rate coefficient, k_{mov} , given by:

$$k_{mov} = \frac{k_{mov0}}{{\phi_P}^5 * \exp\left(k_\eta(\frac{T_g}{T} - 1)\right)} \quad (11)$$

For hemispherical equilibrium morphology, the population balance for aggregates at equilibrium positions can be written as follows:

$$\frac{dn(v)}{dt} = \left(1 - \delta_{v \le 2v_c}\right)\alpha_n(v)\frac{k_a}{V_p}\left(1 - \frac{1}{n_{av}}\right)\int_{v_c}^{v-v_c} n(u)n(v-u)du$$

(Generation by coalescence of aggregates)

$$-2n(v)\frac{k_a}{V_p}\left(1 - \frac{1}{n_{av}}\right)\int_{v_c}^{v_{max}-v} \alpha_n(v+u)n(u)\,du$$

(Disappearance by coalescence of aggregates)

$$+k_{mov}m(v) \quad (12)$$

(Movement to equilibrium)

The population balances should be combined with the material balances for the monomers and polymer that for a batch miniemulsion reaction are as follows:

$$\frac{dM_i}{dt} = -\bar{k}_{p_i}\frac{\bar{n}N_p}{N_A}\frac{M_i}{V_p} \qquad (\frac{mol}{s}) \;;\; M_i(t=0) = M_{i0} \quad (13)$$

$$\frac{dpol}{dt} = \sum -\frac{dM_i}{dt} \qquad (\frac{mol}{s}) \;;\; pol(t=0) = 0 \quad (14)$$

where $\bar{k}_p$ is the average propagation rate coefficient, $\bar{n}$ the average number of radicals per particle, N_p number of particles, N_A is the Avogadro´s number and V_p the total volume of polymer particles given by:

$$V_p = pol\bar{V}_{pol} + \sum_i M_i \bar{V}_{m_i} + V_I \qquad (15)$$

where $\bar{V}_{pol}$ and $\bar{V}_{mi}$ are the average molar volume of the monomer units incorporated into the polymer ($\boldsymbol{\bar{V}_{pol} = \sum_i \varphi_i \bar{V}_{mi}}$) and the monomer molar volumes, respectively, and V_I is the volume of the inorganic nanoparticles.

Equations 1-15 were solved by means of the Kumar-Ramkrishna method[34–36] taking into account the modifications of Butte et al.[37,38] and Calvo et al.[39] The model was implemented in Matlab using 100 pivots running in Windows in a Laptop Intel(R) Core™ i7-4610M CPU @ 3GHz. In the experiments carried out in this work, an inorganic water soluble initiator (KPS) was used. The radicals produced by decomposition of KPS are captured by the polymer particles (after adding some monomer units to become surface active) and the sulfate group of the oligomer anchors the oligoradical to the surface of polymer particle. This leads to a radical concentration profile (methods for the calculation of such profiles are available[40,41]), which strongly affects the particle morphology in the case of polymer-polymer systems.[42] However, it can be demonstrated that the effect of the radical concentration profile on the particle morphology for polymer-inorganic systems prepared by batch miniemulsion polymerization is in most cases weak (if any). In the presence of a sharp radical profile, polymerization mainly occurs at the outer part of the particles. At first sight this might cause a heterogeneous distribution of polymer in the particle, and the

viscosity will be higher in the polymer-rich shell than in the monomer rich core, which will affect the movement of the inorganic material. However, the degree of heterogeneity depends on the ratio between the rate of polymer production that promotes heterogeneity and the rate of monomer-polymer interdiffusion that homogenizes the particle. The calculations presented in the Supporting Information show that the monomer-polymer interdiffusion is much faster than the rate of polymerization. Therefore, the monomer and polymer are homogeneously distributed through the particle and consequently, there is no effect of the radical concentration profile on the movement of the inorganic particles within the polymer particles. In other words, there is no need to consider this profile in the model. Consequently, an average number of radicals per particle ($\bar{n}$ was calculated using the Li-Brooks approach[43]) was used in equations 13 and 14.

Simulation of the morphology of the particles

The model described above was used to simulate the morphology evolution during the miniemulsion polymerization of acrylic/CeO_2 hybrid particles at 60°C as described above. The parameters used in the simulation are given in Table 2. Radical entry and exit rate coefficients were chosen to reach 40% of conversion in 120 minutes, which was the polymerization rate observed experimentally. A monodispersed droplet size was considered and in agreement with the experimental observation, at time = 0, the inorganic nanoparticles (dp=3nm) were uniformly distributed within the monomer droplets forming a stable dispersion. In terms of position, the inorganic particles were considered to be at non-equilibrium position (Figure 1 shows that the final equilibrium morphology was hemispherical).

Table 2. Values of the parameters used in the model.

Parameter	Value	Ref
$k_a(L/s)^*$	20×10^{-23}	This work
$k_{mov}(1/s)^*$	7.2×10^{-4}	This work
N_p	1.26×10^{17}	This work
v_c	1	This work
$k_\eta(kJ/mol)$ **	9	[44]
k	2	[33]
$kp_{\mathrm{MMA}}(L/mol.s)$	$2.67\times10^{6}\exp(-22400/RT)$	[45]
$kp_{\mathrm{BA}}(L/mol.s)$	$2.21\times10^{7}\exp(-17900/RT)$	[46]
r_{MMA}	2.15	[47]
r_{BA}	0.4	[47]
$k_{\mathrm{ads}}(L/mol.s)$	6	This work
$k_{\mathrm{d}}(1/s)$	1×10^{-5}	This work
α*	40	[28]

*model parameters
** for poly(methyl methacrylate)

The outputs of the model are the normalized number and weight distributions of the equilibrium and non-equilibrium clusters; namely m(v) and n(v). In order to compare the predictions of the model with the experimental TEM images, TEM-like images were generated from the distributions. This was carried out by random sampling using the algorithm described in the Supporting Information.

Figures 2-7 compare the simulated and experimental particle morphologies. In these figures, the dark tiny areas represent CeO_2 nanoparticles and the grey area the acrylic (monomer-polymer) matrix. It can be seen that the model captures well the evolution of the particles morphology during polymerization. The inorganic nanoparticles were randomly distributed in monomer droplets (Figure 2). Upon polymerization, the

inorganic nanoparticles tended to aggregate and move toward the equilibrium position. Already in the presence of 1% of polymer (Figure 3), aggregates were formed and a small fraction of these aggregates were at the equilibrium position (surface of the particles). As the polymerization proceeded, bigger and more packed aggregates were formed and the fraction of aggregates at the equilibrium position was higher than at non-equilibrium positions (Figure 4). At 18% of conversion (Figure 5), already most of the particles had one or two aggregates that were mostly placed at the equilibrium position, but still the morphology was not at equilibrium (there were more than one aggregate per particle as an average). At 40% conversion, all the clusters were at equilibrium positions (Figure 6). Finally, at 100% of conversion, the system reached the equilibrium morphology and each particle has an aggregate at the equilibrium position, hemispherical morphology (Figure 7). Note that the simulated images, as well as the experimental TEM images, are a 2D projection of the 3D images, so the aggregates which are located close to the border of the particles, but toward the upper and lower parts of a sphere appeared located in the middle of the circle in the 2D image. The location of CeO_2 aggregates were investigated in detail by 3D-TEM by Aguirre et al.[24] and it was shown that they were at the surface of polymer particles.

a) b)

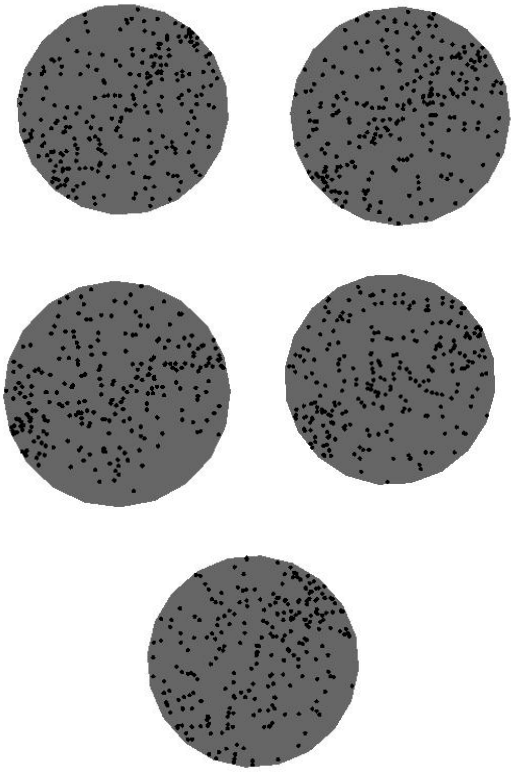

Monomer droplets

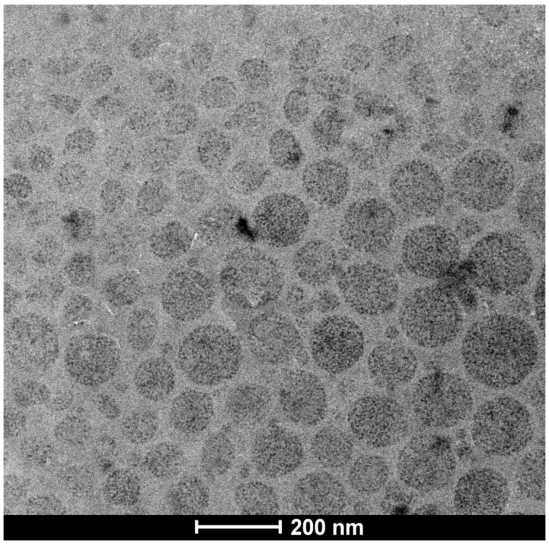

Figure 2. Comparison of the monomer droplets morphology of a hybrid MMA/BA/AA/CeO_2 miniemulsion: a) the morphology predicted by the model and b) Cryo-TEM micrograph of the miniemulsion.

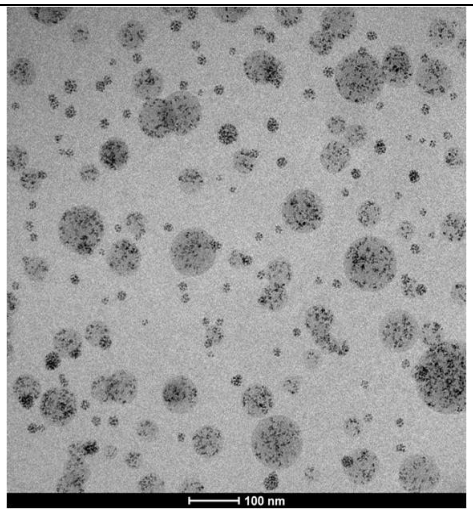

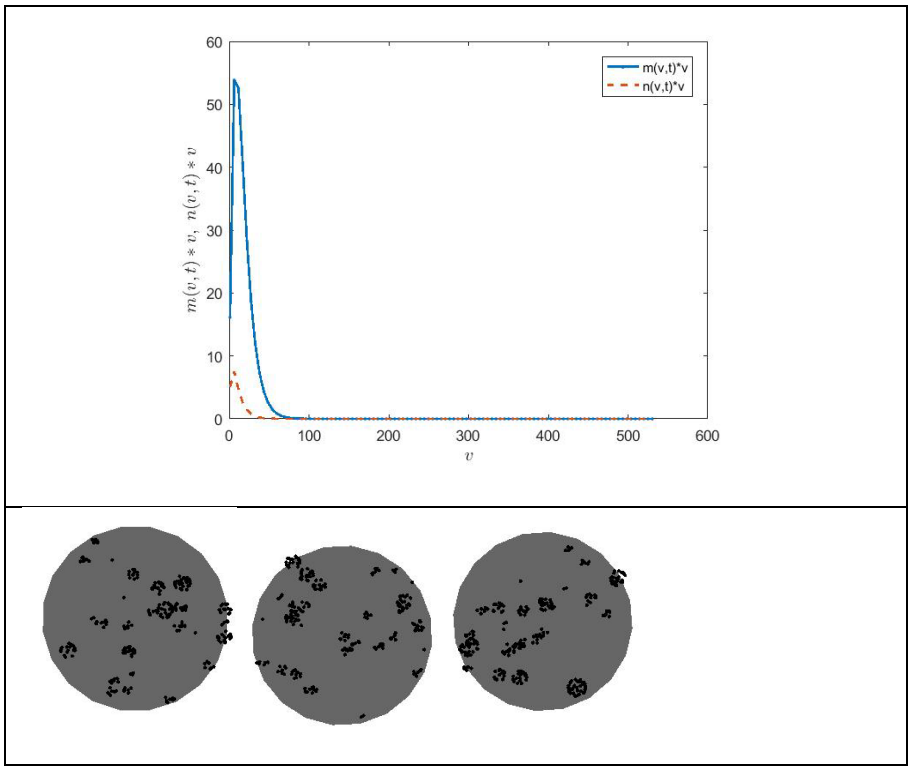

Figure 3. Comparison of the Cryo-TEM micrograph of the polymer particle morphology at X = 1% with the simulated weight distributions (m and n represent aggregates in non-equilibrium and equilibrium positions, respectively) and the TEM-like images obtained from the distributions.

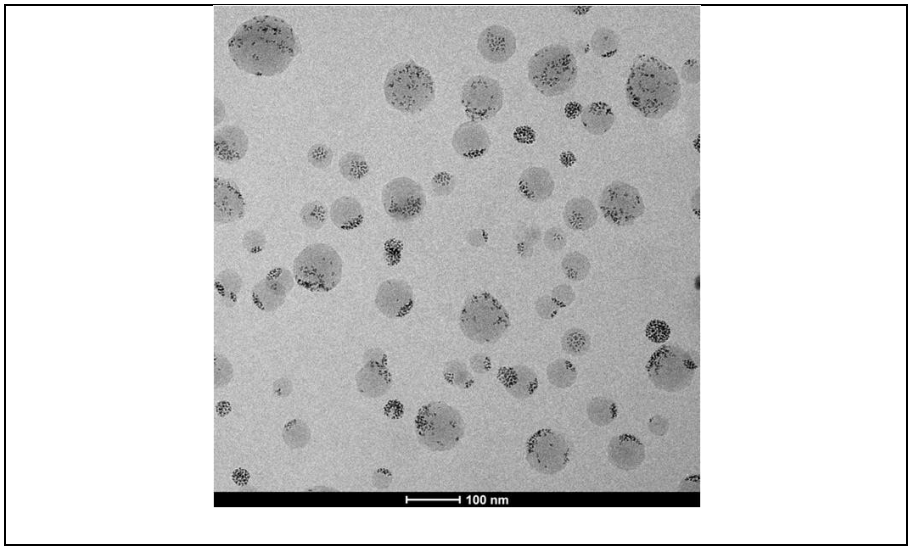

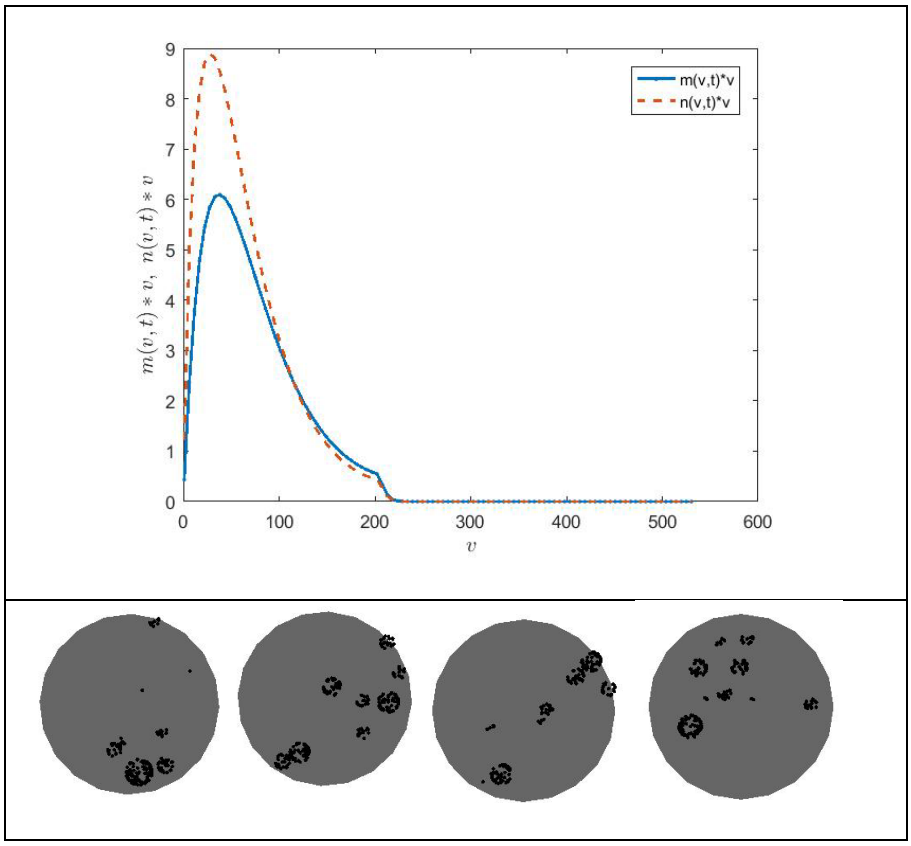

Figure 4. Comparison of the Cryo-TEM micrograph of the polymer particle morphology at X = 8% with the simulated weight distributions (m and n represent aggregates in non-equilibrium and equilibrium positions, respectively) and the TEM-like images obtained from the distributions.

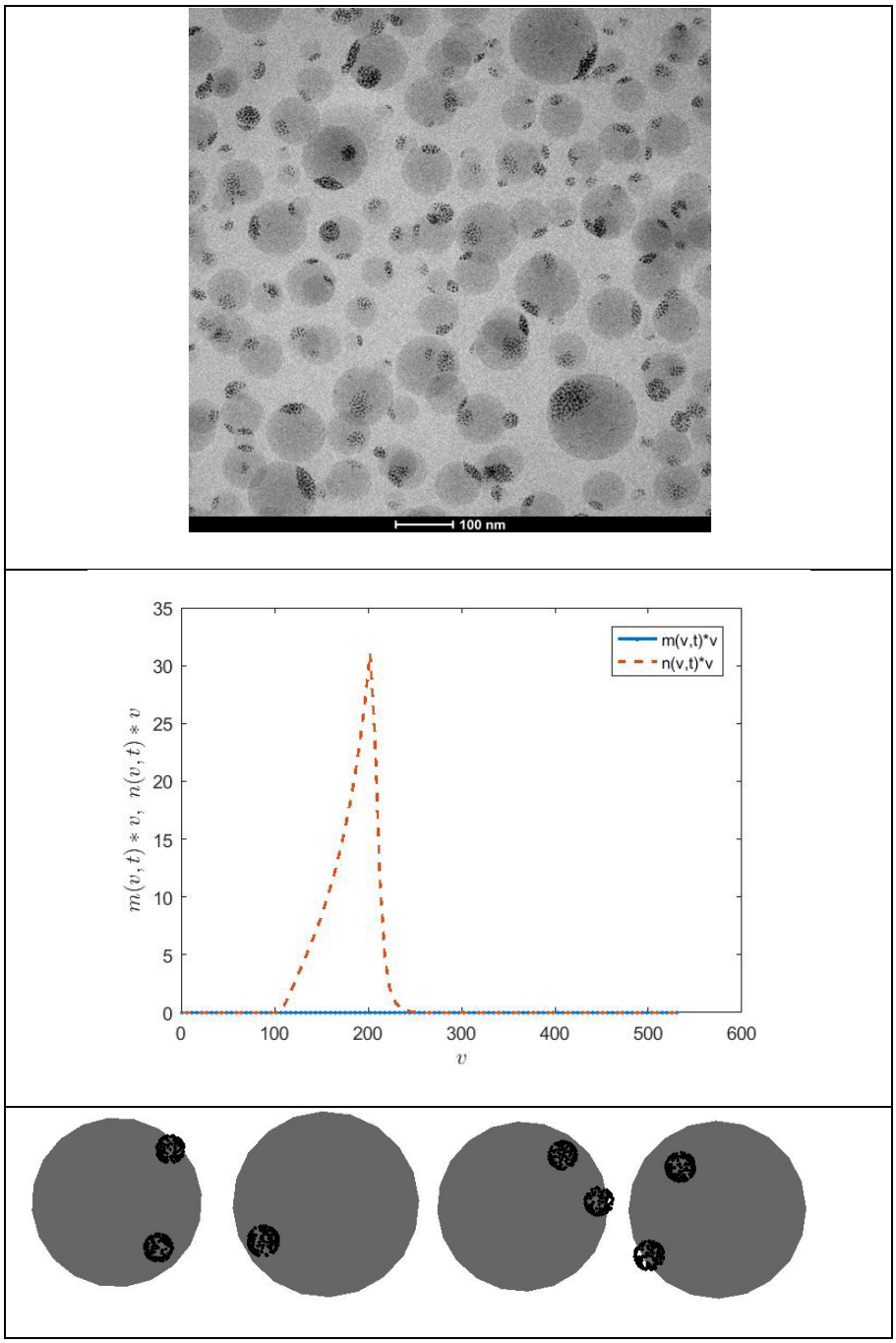

Figure 5. Comparison of the Cryo-TEM micrograph of the polymer particle morphology at X = 18% with the simulated weight distributions (m and n represent aggregates in non-equilibrium and equilibrium positions, respectively) and the TEM-like images obtained from the distributions.

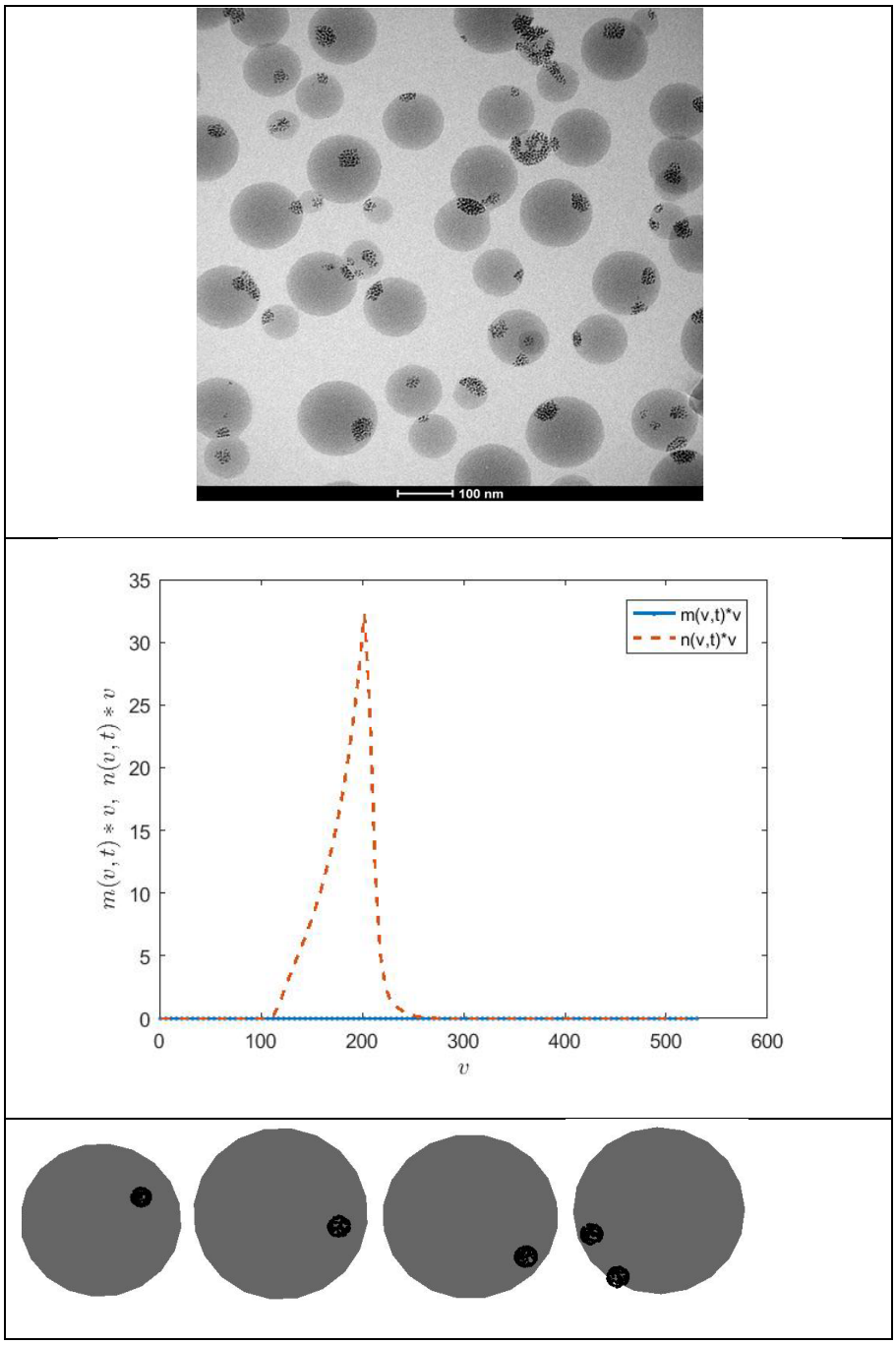

Figure 6. Comparison of the Cryo-TEM micrograph of the polymer particle morphology at X = 40% with the simulated weight distributions (m and n represent aggregates in non-equilibrium and equilibrium positions, respectively) and the TEM-like images obtained from the distributions.

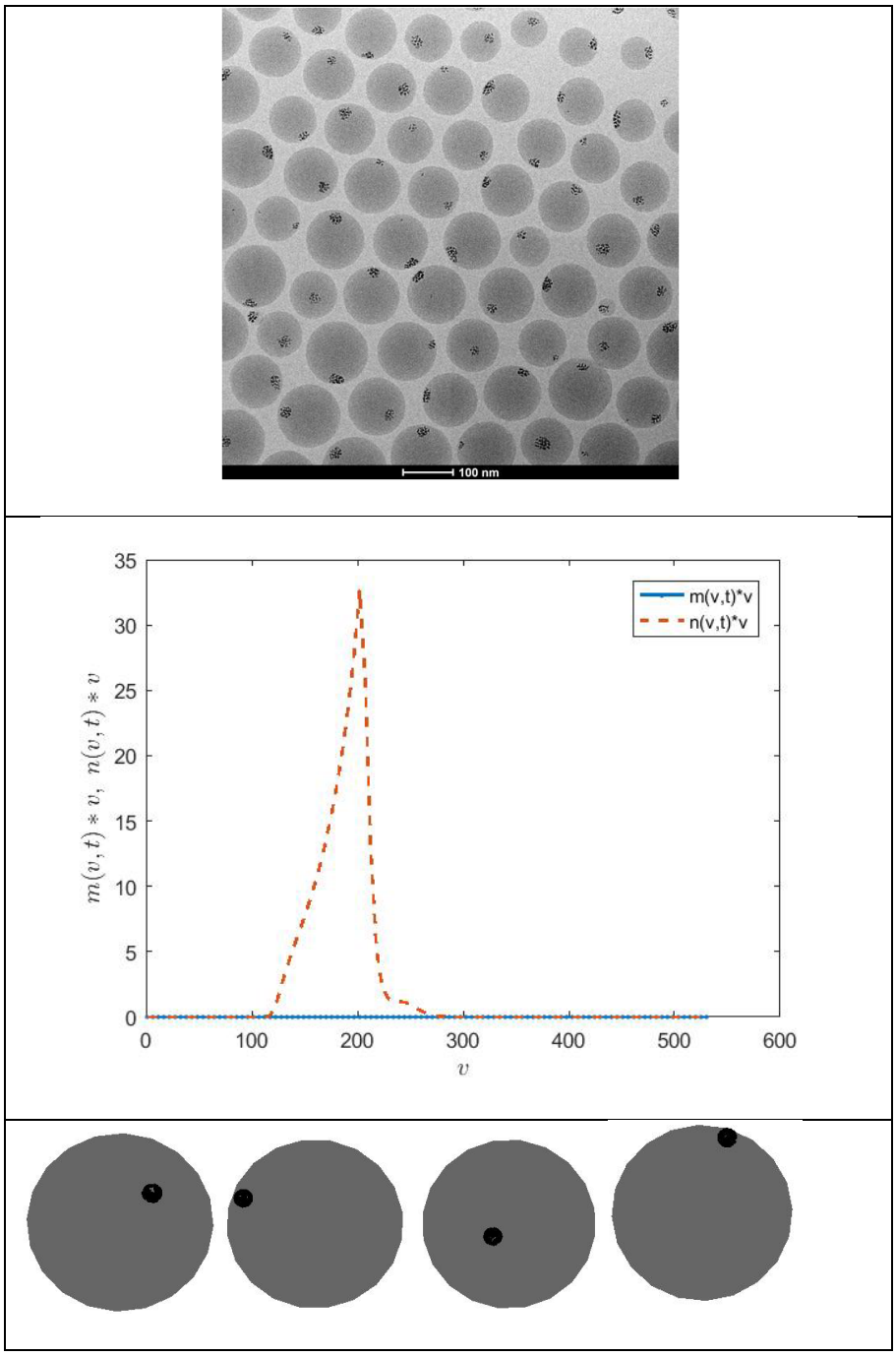

Figure 7. Comparison of the Cryo-TEM micrograph of the polymer particle morphology at X = 100% with the simulated weight distributions (m and n represent aggregates in non-equilibrium and equilibrium positions, respectively) and the TEM-like images obtained from the distributions.

Conclusions

In this work, the evolution of the morphology of polymer-inorganic hybrid particles during their preparation by miniemulsion polymerization of meth(acrylate) monomers in the presence of CeO_2 nanoparticles is investigated. It was found that the morphology evolved from an initial fine dispersion of the CeO_2 nanoparticles within the miniemulsion droplets to a final hemispherical morphology with the CeO_2 nanoparticles forming a compact aggregate placed at the surface of the particles. The evolution was driven by the incompatibility between the hairy layer of the CeO_2 nanoparticles and the newly formed polymer, which even at very low conversions (1%) started the aggregation of the inorganic particles. The experimental results showed non-equilibrium morphologies up to 40% conversion, showing that the particle morphology is the result of the interplay between kinetics and thermodynamics.

A mathematical model for the dynamic evolution of the morphology of polymer-inorganic hybrids was developed and its capabilities to simulate the experimental data were demonstrated.

Acknowledgments

MINECO (CTQ2014-59016-P_and CTQ 2016-80886-R) and the Basque Government (IT999/16) are acknowledged. Miren Aguirre specially acknowledges the financial support obtained through the Post-Doctoral fellowship Juan de la Cierva en Formación (FJCI-2014-22336), from the Ministry of Economy and Competitiveness of Spain.

Nomenclature:

k_p: propagation rate constant

k_a: rate coefficient for cluster coagulation

k_{mov}: movement to equilibrium position rate coefficient

k_{ads}: rate coefficient of entry of radicals to the particles

k_d: rate coefficient of exit of radicals from the particles

M_i: monomer i

$m(v)$: number of clusters with v nanoparticles at non-equilibrium positions

m_{av}: average number of clusters at non equilibrium positions per particle

$n(v)$: number of clusters with v nanoparticles at equilibrium positions

$\bar{n}$: average number of radicals per particle

N_p: number of particles

N_A: Avogadro´s number

n_{av}: average number of clusters at equilibrium position per particle

r_i: reactivity ratio

F_A: van der attraction Waals potential

V_p: total volume of polymer particles

$\bar{V}_{pol}$: molar volume of the polymer

$\bar{V}_{mi}$: molar volume of the monomer *i*

v: number of inorganic nanoparticles in one aggregate

v_c: minimum number of inorganic nanoparticles in one aggregate

v_{max}: maximum number of inorganic nanoparticles in one aggregate

v_{tot}: total number of inorganic nanoparticles in the formulation

α : probability of coagulation of aggregates with number of nanoparticles higher than the average value

η : the internal viscosity of the particle

ϕ_P: the volume fraction of the polymer

k_η : the activation energy for viscous flow

T_g: glass transition temperature

T: polymerization temperature

References

(1) Paulis, M.; Asua, J. M. Knowledge-Based Production of Waterborne Hybrid Polymer Materials. *Macromol. React. Eng.* **2016**, *10*, 8–21.

(2) Xue, Z.; Wieze, H. US Patent, US7094830B2, 2006.

(3) Bourgeat-Lami, E.; Lansalot, M. Organic/Inorganic Composite Latexes: TheMarriage of Emulsion Polymerization and Inorganic Chemistry Elodie. *Adv. Polym. Sci.* **2010**, *233*, 53–123.

(4) González-Matheus, K.; Leal, G. P.; Tollan, C.; Asua, J. M. High Solids Pickering Miniemulsion Polymerization. *Polymer* **2013**, *54*, 6314–6320.

(5) González-Matheus, K.; Leal, G. P.; Asua, J. M. Pickering-Stabilized Latexes with High Silica Incorporation and Improved Salt Stability. *Part. Part. Syst. Charact.* **2014**, *31*, 94–100.

(6) Ma, H.; Luo, M.; Sanyal, S.; Rege, K.; Dai, L. L. The One-Step Pickering Emulsion Polymerization Route for Synthesizing Organic-Inorganic Nanocomposite Particles. *Materials (Basel).* **2010**, *3*, 1186–1202.

(7) Li, K.; Dugas, P. Y.; Lansalot, M.; Bourgeat-Lami, E. Surfactant-Free Emulsion Polymerization Stabilized by Ultrasmall Superparamagnetic Iron Oxide Particles Using Acrylic Acid or Methacrylic Acid as Auxiliary Comonomers. *Macromolecules*

2016, *49*, 7609–7624.

(8) González, E.; Bonnefond, A.; Barrado, M.; Casado Barrasa, A. M.; Asua, J. M.; Leiza, J. R. Photoactive Self-Cleaning Polymer Coatings by TiO2 Nanoparticle Pickering Miniemulsion Polymerization. *Chem. Eng. J.* **2015**, *281*, 209–217.

(9) Yue, L.; Zhang, X. M. Structural Characterization and Photocatalytic Behaviors of Doped CeO2 Nanoparticles. *J. Alloys Compd.* **2009**, *475*, 702–705.

(10) Teixeira, R. F. A.; McKenzie, H. S.; Boyd, A. A.; Bon, S. A. F. Pickering Emulsion Polymerization Using Laponite Clay as Stabilizer To Prepare Armored "Soft" Polymer Latexes. *Macromolecules* **2011**, *44*, 7415–7422.

(11) Bon, S. A. F.; Colver, P. J. Pickering Miniemulsion Polymerization Using Laponite Clay as a Stabilizer. *Langmuir* **2007**, *23*, 8316–8322.

(12) Cauvin, S.; Colver, P. J.; Bon, S. A. F. Pickering Stabilized Miniemulsion Polymerization: Preparation of Clay Armored Latexes. *Macromolecules* **2005**, *38*, 7887–7889.

(13) Nguyen, D.; Zondanos, H. S.; Farrugia, J. M.; Serelis, A. K.; Such, C. H.; Hawkett, B. S. Pigment Encapsulation by Emulsion Polymerization Using Macro-RAFT Copolymers. *Langmuir* **2008**, *24*, 2140–2150.

(14) Ali, S. I.; Heuts, J. P. A.; Hawkett, B. S.; Van Herk, A. M. Polymer Encapsulated Gibbsite Nanoparticles: Efficient Preparation of Anisotropic Composite Latex Particles by RAFT-Based Starved Feed Emulsion Polymerization. *Langmuir* **2009**, *25*, 10523–10533.

(15) Perro, A.; Duguet, E.; Lambert, O.; Taveau, J. C.; Bourgeat-Lami, E.; Ravaine, S. A Chemical Synthetic Route towards "Colloidal Molecules." *Angew. Chemie - Int. Ed.* **2009**, *48*, 361–365.

(16) Zhang, S. W.; Zhou, S. X.; Weng, Y. M.; Wu, L. M. Synthesis of SiO2/Polystyrene Nanocomposite Particles via Miniemulsion Polymerization. *Langmuir* **2005**, *21*, 2124–2128.

(17) Gong, T.; Yang, D.; Hu, J.; Yang, W.; Wang, C.; Lu, J. Q. Preparation of

Monodispersed Hybrid Nanospheres with High Magnetite Content from Uniform Fe3O4 Clusters. *Colloids Surfaces A Physicochem. Eng. Asp.* **2009**, *339*, 232–239.

(18) Ramos, J.; Forcada, J. Surfactant-Free Miniemulsion Polymerization as a Simple Synthetic Route to a Successful Encapsulation of Magnetite Nanoparticles. *Langmuir* **2011**, *27*, 7222–7230.

(19) Aguirre, M.; Paulis, M.; Leiza, J. R. UV Screening Clear Coats Based on Encapsulated CeO2 Hybrid Latexes. *J. Mater. Chem. A* **2013**, *1*, 3155–3162.

(20) Asua, J. M. Mapping the Morphology of Polymer-Inorganic Nanocomposites Synthesized by Miniemulsion Polymerization. *Macromol. Chem. Phys.* **2014**, *215*, 458–464.

(21) Mori, Y.; Kawaguchi, H. Impact of Initiators in Preparing Magnetic Polymer Particles by Miniemulsion Polymerization. *Colloids Surfaces B Biointerfaces* **2007**, *56*, 246–254.

(22) Staudt, T.; Machado, T. O.; Vogel, N.; Weiss, C. K.; Araujo, P. H. H.; Sayer, C.; Landfester, K. Magnetic Polymer / Nickel Hybrid Nanoparticles Via Miniemulsion Polymerization. *Macromol. Chem. Phys.* **2013**, *214*, 2213–2222.

(23) Aguirre, M.; Paulis, M.; Leiza, J. R.; Guraya, T.; Iturrondobeitia, M.; Okariz, A.; Ibarretxe, J. High-Solids-Content Hybrid acrylic/CeO2 Latexes with Encapsulated Morphology Assessed by 3D-TEM. *Macromol. Chem. Phys.* **2013**, *214*, 2157–2164.

(24) Aguirre, M.; Paulis, M.; Barrado, M.; Iturrondobeitia, M.; Okariz, A.; Guraya, T.; Ibarretxe, J.; Leiza, J. R. Evolution of Particle Morphology during the Synthesis of Hybrid acrylic/CeO2 Nanocomposites by Miniemulsion Polymerization. *J. Polym. Sci. Part A Polym. Chem.* **2014**, *53*, 792–799.

(25) Aguirre, M.; Paulis, M.; Leiza, J. R. Particle Nucleation and Growth in Seeded Semibatch Miniemulsion Polymerization of Hybrid CeO2/acrylic Latexes. *Polymer* **2014**, *55*, 752–761.

(26) Asua, J. M. Miniemulsion Polymerization. *Prog. Polym. Sci.* **2002**, *27*, 1283–1346.

(27) Asua, J. M. Challenges for Industrialization of Miniemulsion Polymerization. *Prog.*

Polym. Sci. **2014**, *39*, 1797–1826.

(28) Hamzehlou, S.; Leiza, J. R.; Asua, J. M. A New Approach for Mathematical Modeling of the Dynamic Development of Particle Morphology. *Chem. Eng. J.* **2016**, *304*, 655–666.

(29) González-Ortiz, L. J.; Asua, J. M. Development of Particle Morphology in Emulsion Polymerization. II. Cluster Dynamics in Reacting Systems. *Macromolecules* **1996**, *29*, 383–389.

(30) Hamaker, H. C. The London—van Der Waals Attraction between Spherical Particles. *Physica* **1937**, *4*, 1058–1072.

(31) Gupta, P.; Elkins, C.; Long, T. E.; Wilkes, G. L. Electrospinning of Linear Homopolymers of Poly(methyl Methacrylate): Exploring Relationships between Fiber Formation, Viscosity, Molecular Weight and Concentration in a Good Solvent. *Polymer* **2005**, *46*, 4799–4810.

(32) van Krevelen, D. W.; te Nijenhuis, K. *Properties of Polymers. Their Correlation with Chemical Structure;their Numerical Estimation and Prediction from Additive Group Contributions*, 4th ed.; Elsevier Ltd: Oxford, UK, 2009.

(33) Bueche, F. Rate and Pressure Effects in Polymers and Other Glass-Forming Substances. *J. Chem. Phys.* **1962**, *36*, 2940.

(34) Kumar, S.; Ramkrishna, D. On the Solution of Population Balance Equations by Disretization.I. A Fixed Pivot Technique. *Chem. Eng. Sci.* **1996**, *51*, 1311–1332.

(35) Kumar, S.; Ramkrishna, D. On the Solution of Population Balance Equations by discretization—III. Nucleation, Growth and Aggregation of Particles. *Chem. Eng. Sci.* **1997**, *52*, 4659–4679.

(36) Kumar, S.; Ramkrishna, D. On The Solution Of Population Balance Equations By Discritization-II. A Moving Pivot Technique. *Chem. Eng. Sci.* **1996**, *2114*, 1333–1342.

(37) Butte, A.; Storti, G.; Morbidelli, M. Evaluation of the Chain Length Distribution in Free-Radical Polymerization,1 Bulk Polymerization. *Macromol. Theory Simul.* **2002**,

11, 22–36.

(38) Butte, A.; Storti, G.; Morbidelli, M. Evaluation of the Chain Length Distribution in Free-Radical Polymerization , 2 Emulsion Polymerization. *Macromol. Theory Simulations* **2002**, *11*, 37–52.

(39) Calvo, I.; Hester, K.; Leiza, J. R.; Asua, J. M. Mathematical Modeling of Carboxylated SB Latexes. *Macromol. React. Eng.* **2014**, *8*, 329–346.

(40) Chern, C. S.; Poehlein, G. W. Polymerization in Nonuniform Latex Particles: Distribution of Free Radicals. *J. Polym. Sci. Part A-Polymer Chem.* **1987**, *25*, 617–635.

(41) de La Cal, J. C.; Urzay, R.; Zamora, A.; Forcada, J.; Asua, J. M. Simulation of the Latex Particle Morphology. *J. Polym. Sci. Part A Polym. Chem.* **1990**, *28*, 1011–1031.

(42) Stubbs, J.; Karlsson, O.; Jönsson, J.-E.; Sundberg, E.; Durant, Y.; Sundberg, D. Non-Equilibrium Particle Morphology Development in Seeded Emulsion Polymerization. 1: Penetration of Monomer and Radicals as a Function of Monomer Feed Rate during Second Stage Polymerization. *Colloids Surfaces A Physicochem. Eng. Asp.* **1999**, *153*, 255–270.

(43) Li, B.-G.; Brooks, B. W. Prediction of the Average Number of Radicals per Particle for Emulsion Polymerization. *J. Polym. Sci. Part A Polym. Chem.* **1993**, *31*, 2397–2402.

(44) Krevelen, V.; Hoftyzer, P. J. Newtonian Shear Viscosity of Polymeric Melts. *Die Angew. Makromol. Chemie* **1976**, *52*, 101–109.

(45) Beuermann, S.; Buback, M.; Davis, T. P.; Gilbert, R. G.; Hutchinson, R. A.; Olaj, O. F.; Russell, G. T.; Schweer, J.; van Herk, A. M. Critically Evaluated Rate Coefficients for Free-Radical Polymerization, 2. Propagation Rate Coefficients for Methyl Methacrylates. *Macromol. Chem. Phys.* **1997**, *198*, 1545–1560.

(46) Asua, J. M.; Beuermann, S.; Buback, M.; Castignolles, P.; Charleux, B.; Gilbert, R. G.; Hutchinson, R. A.; Leiza, J. R.; Nikitin, A. N.; Vairon, J. P.; et al. Critically

Evaluated Rate Coefficients for Free-Radical Polymerization, 5 Propagation Rate Coefficient for Butyl Acrylate. *Macromol. Chem. Phys.* **2004**, *205*, 2151–2160.

(47) Van Herk, A. M. Pulsed Initiation Polymerization as a Means of Obtaining Propagation Rate Coefficients in Free-Radical Polymerizations. II Review up to 2000. *Macromol. Theory Simulations* **2000**, *9*, 433–441.

"For table of contents only"

Table of Contents Graphic

Dynamics of the particle morphology during the synthesis of waterborne polymer-inorganic hybrids

*Shaghayegh Hamzehlou; Miren Aguirre; Jose R. Leiza; José M. Asua**